# Improvement of the quantum confined Stark effect characteristics by means of energy band profile modulation: The case of Gaussian quantum wells

A. Ramírez-Morales, J. C. Martínez-Orozco, and I. Rodríguez-Vargas

Citation: Journal of Applied Physics **110**, 103715 (2011); doi: 10.1063/1.3662907
View online: https://doi.org/10.1063/1.3662907
View Table of Contents: http://aip.scitation.org/toc/jap/110/10
Published by the American Institute of Physics

**Articles you may be interested in**

Electronic structure computation and differential capacitance profile in δ-doped FET as a function of hydrostatic pressure
AIP Conference Proceedings **1598**, 222 (2014); 10.1063/1.4878313

Angle-dependent transmission in graphene heterojunctions
Applied Physics Letters **106**, 013112 (2015); 10.1063/1.4905566

Resonant tunneling through double barrier graphene systems: A comparative study of Klein and non-Klein tunneling structures
Journal of Applied Physics **112**, 073711 (2012); 10.1063/1.4757591

Angle-dependent bandgap engineering in gated graphene superlattices
AIP Advances **6**, 035309 (2016); 10.1063/1.4944495

MBE-grown 232–270 nm deep-UV LEDs using monolayer thin binary GaN/AlN quantum heterostructures
Applied Physics Letters **110**, 041108 (2017); 10.1063/1.4975068

Short-wave infrared (λ = 3 μm) intersubband polaritons in the GaN/AlN system
Applied Physics Letters **110**, 131102 (2017); 10.1063/1.4979084

AIP Journal of Applied Physics SPECIAL TOPICS LEARN MORE

# Improvement of the quantum confined Stark effect characteristics by means of energy band profile modulation: The case of Gaussian quantum wells

A. Ramírez-Morales, J. C. Martínez-Orozco, and I. Rodríguez-Vargas[1,a)]
*Unidad Académica de Física, Universidad Autónoma de Zacatecas, Calzada Solidaridad Esquina Con Paseo La Bufa S/N, 98060 Zacatecas, Zac., México*

(Received 19 August 2011; accepted 17 October 2011; published online 29 November 2011)

We study the quantum confined stark effect (QCSE) characteristics in Gaussian quantum wells (GQW). This special energy band profile is built varying the aluminum concentration of the AlGaAs ternary alloy in Gaussian fashion. The semi-empirical $sp^3s^*$ tight-binding model including spin is used to obtain the energy Stark shifts (ESS) and the wave-function Gaussian spatial overlap (GSO) between electrons and holes for different electric field strengths, quantum well widths and aluminum concentrations. We find that both the ESS and the GSO depend parabolically with respect to the electric field strength and the quantum well width. These QCSE characteristics show an asymmetry for the electric field in the forward and reverse directions, related directly to the different band-offset of electrons and holes, being the negative electric fields (reverse direction) more suitable to reach greater ESS. Two important features are presented by this special energy band profile: (1) reductions of the ESS and (2) enhancements of the GSO of tents to hundreds with respect to parabolic and rectangular quantum wells. Even more, tailoring the quantum well width it is possible to reach GSO of thousands with respect to rectangular quantum wells. Finally, it is important to mention that similar results could be obtained in other quantum well heterostructures of materials such as nitrides, oxides (ZnO), and SiGe whenever the confinement band profiles are modulated in Gaussian form. © *2011 American Institute of Physics*. [doi:10.1063/1.3662907]

## I. INTRODUCTION

Quantum confined stark effect (QCSE), the analog of the Franz-Keldysh effect for uniform bulk semiconductors and the Stark-effect for atoms, is an effect that arises when an electric field is applied along the growth direction of a quantum well (QW) heterostructure.[1] There are two important characteristics of the QCSE: (1) a redshift of the energy of the confined electron-hole pairs that results in a energy Stark shift (ESS) in the excitonic absorption and (2) a reduction of the oscillator strength and consequently a diminishing of the transition probabilities. Both characteristics result from the separation of electrons and holes toward opposite sides of the quantum well. As a result of such properties and the high internal quantum efficiency (IQE) of quantum well structures made from III to V semiconductors such as GaAs and InP and their alloys,[1–5] the QCSE has been widely used in electroabsorption modulators for telecommunications.[6] However, these III-V materials are difficult to integrate with electronic devices made mainly with silicon. A relative new and interesting proposal for silicon photonics[7] is reported by Kuo and colleagues.[8] They have demonstrated efficient QCSE characteristics in silicon-based structures using strained Ge multiple quantum wells. These characteristics resemble those of III-V materials with the difference that the materials and fabrication processes reported are totally compatible with the complementary metal-oxide semiconductor (CMOS) technology.

Currently, there is also a lot of interest in reduce and control the QCSE in solid state lighting (SSL) applications based on light emitting diodes (LEDs). These devices are made mainly on materials that present internal electric fields, as a result of strain-induced spontaneous and piezoelectric polarization, such as Nitrides[9–15] (InGaN/GaN, GaN/AlGaN, etc.) and recently on Oxides[16–21] (ZnO/ZnMgO). In particular, InGaN-based quantum well devices present numerous effects such as bandgap narrowing, blueshift of photoluminescence with increasing excitation, modification of the oscillator strength for carriers, and nonuniform carrier distribution. Effects that in most cases affects the efficacy and efficiency (green gap and efficiency droop) of SSL devices. A common factor in all mentioned effects is the QCSE, becoming the control of the latter a key technical issue of critical importance in the improvement of SSL devices. The different proposals to mitigate the QCSE in InGaN-based quantum wells can be categorized as: (a) QCSE screening by doping, (b) nonpolar epitaxial structures, (c) strain, field, and band engineering, and (d) cubic nitride structures. However, all these possibilities have endemic problems as for example blocking effects of hole transport by Si doping, the extremely high cost and tiny size of the substrates available for the nonpolar and semipolar SSL devices and the high cost of mass production of the cubic-phase nitride materials for mention a few. For more details, the interested reader can see the excellent review of Ryou and colleagues[15] (and references cited therein).

Recently, another possibility based on the modulation of the energy band profile of a quantum well has been investigated.[22–28] The main idea is to change the energy band profile of electrons and holes by means of doping, staggering and grading of the quantum wells in such a way that

a)Electronic mail: isaac@fisica.uaz.edu.mx.

 © 2011 American Institute of Physics

the electron and hole overlap increases. Graded quantum wells seem to be reasonable if we take into account the excellent experimental control that offers the current growth techniques to obtain these structures. Han *et al.*[28] have demonstrated experimentally that multiple quantum well light-emitting diodes with trapezoidal wells improve efficiency droop at high current densities. The improvement is attributed to the increase of the IQE that result from a better electron-hole overlap. From a theoretical stand point Wang *et al.*[26] and Yang *et al.*[27] have investigated graded quantum well LEDs. They found spontaneous emission rates of asymmetrically graded quantum wells three times larger than rectangular case for various carrier densities[26] as well as improvement of optical gain and higher polarization degree in triangular shaped quantum well.[27]

In this work, we study theoretically the differences of the QCSE characteristics of the Gaussian quantum wells (GQWs) with respect to the parabolic (PQWs) and rectangular ones (RQWs). We aim to understand how this special energy band profile (GQWs) influences the mentioned characteristics for different applied electric fields and quantum well widths. For this purpose we study a simple but illustrative III-V AlGaAs system for which the aluminum concentration is varied in Gaussian, parabolic, or rectangular form resulting in energy band profiles of the same shape of the aluminum concentration.

## II. METHODOLOGY

The quantum well system we are interested in is composed of two homogeneous AlGaAs regions of fix aluminum concentration (reference concentration) that sandwiched an inhomogeneous region with varying aluminum concentration. The aluminum concentration of the inhomogeneous region is varied according to a specific functional rule, in our particular case of Gaussian form which turns out in conduction and valence band edges with the same functional dependence, Fig. 1(a), due to the linear relation between the energy band-edge and the aluminum concentration. If an electric field is applied along the growth direction of the inhomogeneous slab the resulting energy band-edge profiles for electrons and holes will tilt due to the linear dependence of the external potential with respect to the applied electric field and the growth direction, Fig. 1(b).

We have treated the mentioned system within the lines of the semi-empirical $sp^3s^*$ tight-binding model including spin.[29–31] The surface green function matching method (SGFM) (Ref. 32) and the transfer matrix[33] approach have been used to obtain the electronic structure through the relation between the local density of sates (LDOS) and the Green Function

$$LDOS(E,\kappa,n) = -\frac{1}{\pi}\,\mathrm{Im\ Tr}\ G(E,\kappa,n), \tag{1}$$

where the Green Function $G$ can be obtained knowing the Green Functions of the homogeneous regions and the inhomogeneous slab together with the matching formulae. In this case, $n$ numbers the principal layer or mono layer (ML). A ML consists of a layer of anions and cations and is approximately 2.825 Å. $\kappa$ is the two-dimensional wave vector $(k_x, k_y)$ and the energy $E$ is understood in the causal sense $E \to E + i\epsilon$ with $\epsilon \to 0$. We have projected the LDOS at the center of the Brillouin zone $\kappa = 0$ as well as at the center of the inhomogeneous slab. Likewise, we have considered the imaginary part of the energy as $10^{-4}$ eV. This is done for three main reasons: (1) to reduce the computational-time

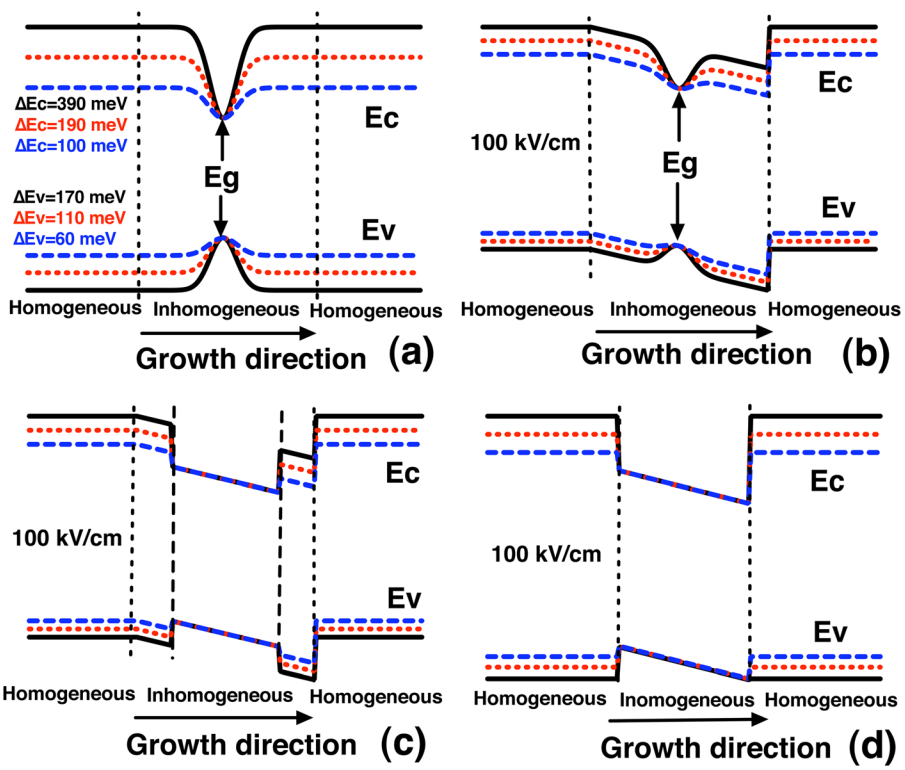


FIG. 1. (Color online) (a) Energy band diagram of our AlGaAs Gaussian quantum well system consisting of an inhomogeneous region of varying aluminum concentration in Gaussian form sandwiched between two homogeneous semi-infinite slabs of fix aluminum concentration (reference concentration) along the growth direction (z). (b) The same as in (a) but now considering an applied electric field along the growth direction. The applied electric field acts only in the inhomogeneous slab. (c) Electron and hole energy band-edge profiles of RQWs under an applied electric field. In this case, the inhomogeneous slab consists of a quantum well region sandwiched between two barrier regions, regions between the dotted and dashed vertical lines. (d) The simplification of (c) neglecting the barrier regions between the dotted and dashed vertical lines. In all cases the solid-black, dotted-red, and dashed-blue lines state aluminum reference concentrations of 0.3, 0.2, and 0.1, respectively.

cost; (2) to avoid homogeneous barrier effects; and (3) to maximize the spectral strength of electron and hole states. In all cases treated in the present work, we adopt this kind of criteria. The energy band-edge profile modulation is taking into account by means of the appropriate modification of the tight-binding parameters as function of the aluminum concentration.

In the case of the constant electric field applied in the growth direction, we have used the reasonable and good approximation proposed by Graf and Vogl.[34] This approximation consists in the modification of all diagonal elements of the tight-binding Hamiltonian matrix in each atomic layer

$$TB_{ii}(n) = TB_{ii}(0) + neF, \tag{2}$$

where $n$ labels the atomic layers in the growth direction, $e$ is the electron charge, $F$ is the magnitude of the constant electric field, and $TB_{ii}$ are the diagonal tight-binding parameters.

## III. RESULTS AND DISCUSSION

In Fig. 1(c), the original inhomogeneous slab that consists of two barriers (regions between dotted and dashed vertical lines) and a quantum well region has been changed by an equivalent quantum well system without barriers (simplified system) as can be seen in Fig. 1(d). The applied electric field acts only in the inhomogeneous slab. The fix aluminum concentration in the semi-infinite homogeneous slabs has been taken as reference value to identify the different quantum well systems treated in the present work. The solid-black, dotted-red, and dashed-blue correspond to reference concentrations $x = 0.3$, $x = 0.2$, and $x = 0.1$. The goal of this simplification is to readily and clearly identify the electron and hole ground states in the LDOS outputs without sacrifying accuracy and reliability of the results. To check out that this change is good, we have calculated the ESS and spatial overlap of the electron and hole ground states for the GQWs, PQWs, and RQWs (results not shown), and we find practically no change in the ESS between the original and the simplified system. In the case of the relative spatial overlap (RSO), this is the ratio of the spatial overlap between electron and hole ground states of GQWs to PQWs (RSOGP) and GQWs to RQWs (RSOGR) the differences between original and simplified wells are barely perceptible, especially in the high field limit. From now on, we will deal with the simplified system, even when we not refer to it explicitly.

In Fig. 2(a), we show the energy Stark shifts as function of the applied electric field strength for GQWs (red lines), PQWs (blue lines), and RQWs (black lines). We have fixed the quantum well width (dw) at 60 MLs for three different aluminum concentrations $x = 0.3$ (solid line), $x = 0.2$ (dotted line), and $x = 0.1$ (dashed line). The ESS of all quantum well systems present a quadratic dependence with respect to the applied electric field being the main difference the fitting parameters of the respective curves. In the case of the RQWs, the fitting parameters are 4.74E-3, 4.87E-3, and 5.16E-3, for PQWs 1.7E-3, 2.46E-3, and 4.72E-3, and for GQWs, we have 3.52E-4, 1.15E-3, and 2.53E-3 corresponding to the three aluminum concentrations $x = 0.3$, $x = 0.2$, and $x = 0.1$ in each case. The maximum ESS reached for RQWs, PQWs,

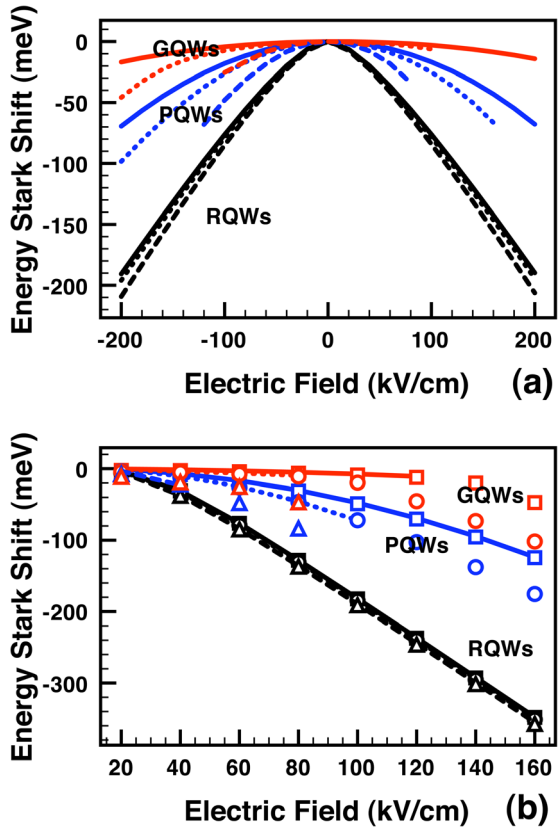


FIG. 2. (Color online) Energy Stark shifts for the different quantum well systems: (Red) GQWs, (Blue) PQWs, and (Black) RQWs. (a) ESS as function of F with $dw = 60$ MLs and $x = 0.3$, 0.2, and 0.1 solid, dotted, and dashed lines, respectively. (b) ESS versus dw fixing F at 100 kV/cm (line graph) and −100 kV/cm (symbol graph). The solid, dotted, and dashed lines correspond to $x = 0.3$, 0.2, and 0.1 in the case of $F = 100$ kV/cm. Likewise, for the squares, circles, and triangles but for $F = -100$ kV/cm.

and GQWs are 200 meV, 100 meV, and 50 meV, respectively. These values are reached for the maximum negative electric field considered and concentration $x = 0.2$ in the case of PQWs and GQWs, meanwhile for RQWs all concentrations work well for both negative and positive electric fields. Other interesting feature is the equivalence of ESS that the GQWs ($x = 0.3$) and PQWs ($x = 0.2$) show for negative electric fields up to −100 kV/cm pointing out that these quantum well systems behave in the same way in this particular case. The ESS also present an evident asymmetry with respect to the applied electric field, particularly the GQWs and PQWs at aluminum concentrations $x = 0.2$ and $x = 0.1$. We can attribute this asymmetry to two factors: (1) the smaller attractiveness of the GQWs and PQWs with respect to the RQWs and (2) the enhancement or diminishment of the electron and hole localizations depending on the sign of the electric field. The first factor comes from the special form of the energy band-edge profiles of GQWs and PQWs, and the second from the disproportion of the band-offset between electron and holes, see Fig. 1(a). In the case of positive electric fields, the localization (delocalization) of electrons (holes) is enhanced (diminished) with opposite trend for negative electric fields. Taking into account that the energy band-edge confinement of electrons is nearly twice of the holes turns out that the latter are totally delocalized for

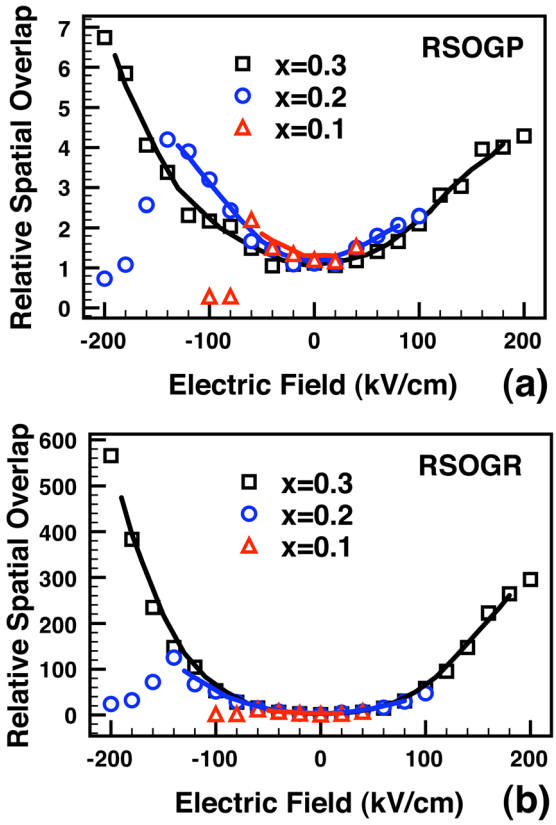


FIG. 3. (Color online) Relative spatial overlap of GQWs as function of the electric field strength. In particular, spatial overlap ratio between (a) GQWs and PQWs and (b) GQWs and RQWs, respectively. The black-squares, blue-circles, and red-triangles correspond to x = 0.3, 0.2, and 0.1 with the same well width, dw = 60 MLs. The lines represent the best fitting (interpolation) of our data.

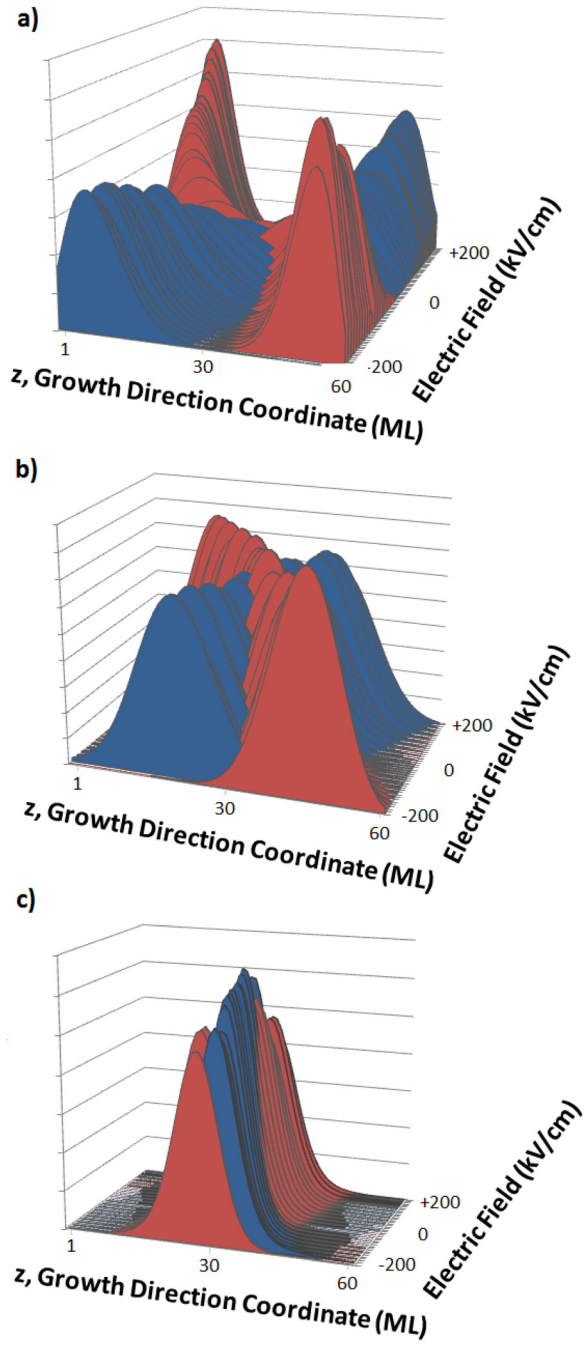


FIG. 4. (Color online) Three-Dimensional graphs of the spatial overlap between the electron and hole ground state wave-functions for (a) RQWs, (b) PQWs, and (c) GQWs. The z, y, and x axis represent the spectral strength (a.u.), growth direction (MLs), and the electric field (kV/cm). The blue and red curves correspond to electrons and holes, respectively. In this case, the aluminum concentration and well width are fixed to 0.3 and 60 MLs.

small positive electric fields at small aluminum concentrations, even for negative electric fields with x = 0.1 electrons reach delocalization at fields of −100 kV/cm and −120 kV/cm for GQWs and PQWs, respectively.

Similar trend is obtained for ESS as function of the quantum well width, Fig. 2(b). We have fixed the applied electric field at 100 kV/cm (line graphs) and −100 kV/cm (symbol graphs). The red, blue and black curves represent GQWs, PQWs, and RQWs. The solid (square), dotted (circle), and dashed (triangle) curves correspond to x = 0.3, x = 0.2, and x = 0.1. The maximum ESS reached for GQWs, PQWs, and RQWs are 100 meV, 175 meV, and 350 meV, respectively. These values are reached for negative electric field at maximum well width considered 160 MLs. There is also asymmetry of the ESS with respect to the sign of the electric field being the Gaussian and parabolic quantum well systems which sustain this feature. The ESS of GQWs (x = 0.1) and PQWs (x = 0.2) match perfectly up to 80 MLs. Delocalization effects are more pronounced for positive electric fields, in GQWs and PQWs, presenting it even for narrow quantum wells. In this case, the fitting parameters for x = 0.3, x = 0.2, and x = 0.1 of RQWs are 1.36E-2, 1.37E-2, and 1.39E-2, for PQWs are 4.83E-3, 6.85E-3, and 1.31E-2, and for GQWs are 1.84E-3, 3.97E-3, and 7.32E-3.

Figure 3 shows the GSO versus the applied electric field. Particularly, we have calculated the ratio of spatial overlap between GQWs and PQWs as well as between GQWs and RQWs, Figures 3(a) and (b). The quantum well width of all systems has been remained fix at 60 MLs. The black-squares, blue-circles, and red-triangles correspond to aluminum concentrations of 0.3, 0.2, and 0.1. As in the case of ESS, the RSO shows a quadratic dependence with respect to the electric field. This dependence can be attributed to the special form of the GQWs since the spatial overlap between the wave functions of the electron and hole ground states is

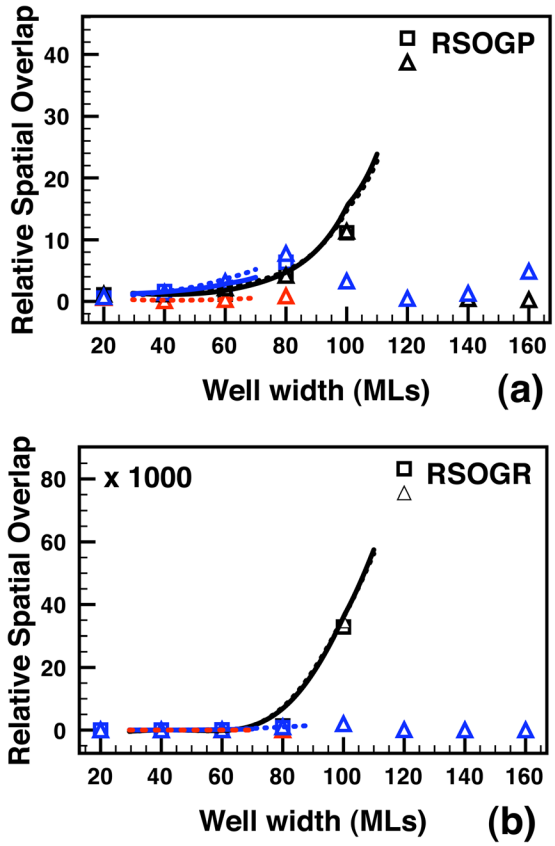


FIG. 5. (Color online) Relative spatial overlap of GQWs versus the quantum well width. In particular, spatial overlap ratio between (a) GQWs and PQWs and (b) GQWs and RQWs, respectively. The black, blue, and red squares (triangles) correspond to $x = 0.3$, 0.2, and 0.1 with $F = 100$ kV/cm ($-100$ kV/cm). The solid and dotted lines represent the best fitting (interpolation) of our data.

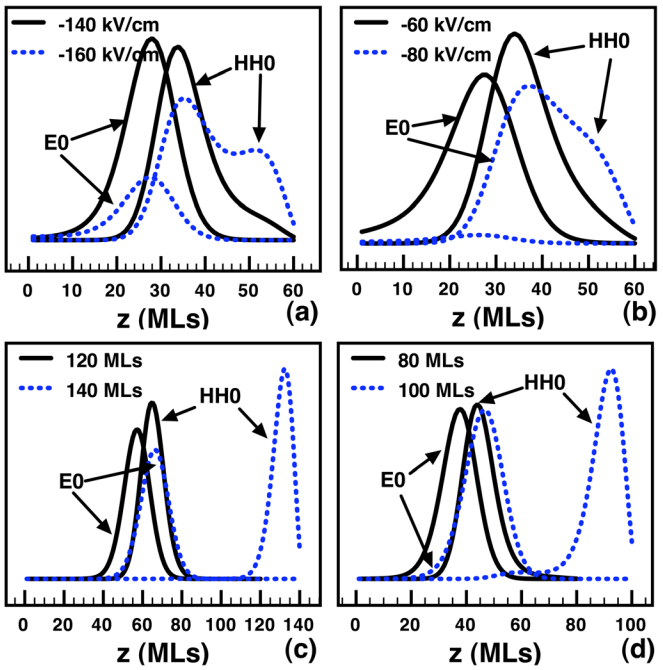


FIG. 6. (Color online) Spatial distribution of the electron and hole ground states of GQWs for (a) $x = 0.2$ and (b) $x = 0.1$ at the inflection points of the relative overlap of Fig. 3 as well as for (c) $x = 0.3$ and (d) $x = 0.2$ at the inflection points of the relative overlap of Fig. 5. In the case of (a), these points correspond to $-140$ kV/cm and $-160$ kV/cm, meanwhile for (b) to $-60$ kV/cm and $-80$ kV/cm. Likewise, (c) is referring to 120 MLs and 140 MLs, and (d) to 80 MLs and 100 MLs, respectively. The solid-black (dotted-blue) lines represent the electron and hole states prior (after) the inflection.

less sensitive to the electric field meanwhile the wave functions of electrons and holes of RQWs readily apart each other to opposite sides of the quantum well resulting in a rapid reduction of the spatial overlap, see Fig. 4. The PQWs are an intermediate case with better spatial overlap than RQWs but worse with respect to GQWs. All this is reflected in the vertical axis of RSO with improvement factors up to 7 and 500 for RSOGP and RSOGR, respectively. The asymmetry of the RSO can be understood in terms of the disproportion of band-offset between electrons and holes, with the negative electric field more appropriate to reach higher RSO. Another interesting characteristic of the RSO is the inflection point at $-160$ kV/cm and $-60$ kV/cm for $x = 0.2$ and $x = 0.1$, respectively. This point is the same for both RSOGP and RSOGR which means that it is totally related to the spatial overlap of the Gaussian wells. Figures 6(a) and (b) show the spatial distribution of the electron and hole ground states prior and after the inflection, we can see clearly that the lower spatial overlap at $-160$ kV/cm and $-80$ kV/cm is caused mainly by the lower electron localization, which is more dramatic at $-80$ kV/cm ($x = 0.1$).

RSO of GQWs varying the quantum well width is shown in Fig. 5. The applied electric field has been fixed at 100 kV/cm (squares) and $-100$ kV/cm (triangles). The black, blue, and red curves correspond to $x = 0.3$, $x = 0.2$, and $x = 0.1$. As in the case of Fig. 3, we see a quadratic-like dependence, however, in this case, the RSO remains practically unchanged up to 80 MLs (100 MLs), for RSOGP (RSOGR), Fig. 5(a) (Fig. 5(b)), reaching its maximum value at 120 MLs. For negative applied electric field and $x = 0.3$, there is drastic drop from 120 MLs to 140 MLs which we can attribute, contrary to RSO versus $F$, to the localization of the electron and hole wave functions on opposite sides of the Gaussian quantum well, Fig. 6(c). Similarly for $x = 0.2$ with maximum at 80 MLs and drop at 100 MLs, Fig. 6(d). Interesting to note is the factors involved at the maximum for $x = 0.3$ with values of 40 and 80 000 for RSOGP and RSOGR which mean that tailoring the well width it is possible to reach sizable RSO. Wide quantum wells, 140 MLs and 160 MLs, also present an increase of the RSOGP that can be attributed to the higher drop of spatial overlap of the PQWs rather than an increase of the overlap of GQWs. Moreover, at these well widths, both quantum well systems sustain negligible spatial overlap.

Likewise, we want to mention that our findings obey the same tendency observed or theoretically predicted in other quantum well systems with asymmetrical, triangular, and trapezoidal energy band profiles.[26–28] For instance, Wang *et al.*[26] have investigated theoretically the asymmetrically graded InGaN/GaN QW turning out that the energy band profile becomes parabolic-like due to the increase of the internal electric field along the growth direction. The momentum-matrix elements of the electron-hole ground state transition are 3.5 times larger than those in rectangular

QW due to the larger overlap of graded QW, which implies larger spontaneous emission rate of graded QW as well. Similarly, Yang *et al.*[27] have studied the electron-hole wavefunction overlap and optical gain characteristics of triangular InGaN quantum wells. They found that this special energy band profile exhibits higher overlap of electrons and holes wave functions as well as remarkable increase in both optical gain and polarization degree. Han *et al.*[28] have grown InGaN/GaN multiple quantum well LEDs on a sapphire substrate. They performed a comparative study preparing conventional rectangular QW LEDs and trapezoidal QW LEDs. They found that LEDs with trapezoidal wells show a lower forward voltage and an external quantum efficiency 20% higher compared to LEDs with rectangular wells resulting in improvement of the efficiency droop at high current densities which is mainly due to the enhancement of the overlap of the electron and hole wave functions.

As a final remark, it is important to mention that the GQWs, particularly, those for the higher aluminum concentration considered $x = 0.3$, are less affected by the QCSE. This is, the ESS remain practically unchanged over the whole range of electric fields considered as well as the RSO, to our knowledge, sustain the larger values ever reported which implies that LEDs with GQWs will show better stability of emission wavelength in operation. We also hope that the present study be stimulating for our experimental counterparts in order to build quantum well systems with energy band profiles of Gaussian form.

## IV. CONCLUSIONS

In summary, the QCSE characteristics of AlGaAs Gaussian quantum wells are studied theoretically by the semiempirical $sp^3s^*$ tight-binding model including spin. The aluminum concentration in the AlGaAs ternary alloy is varied Gaussianly turning out in a energy band profile of Gaussian form for both electrons and holes. It is found that irrespective of the form of the energy band profile (Gaussian, parabolic, or rectangular) the QCSE characteristics show quadratic dependence with respect to the electric field strength and the quantum well width. In addition, the different band-offset of electrons and holes results in an asymmetry of the ESS and GSO under a change of direction of the applied electric field, being the negative electric field more appropriate to reach higher ESS and GSO for fix quantum well width and aluminum concentration. The special form of the Gaussian quantum wells turns out in substantial reductions and enhancements of the ESS and GSO with respect to PQWs and RQWs. For instance, reduction (enhancement) factors of tens and hundreds can be reached for ESS (GSO), even more it is possible to obtain factors of thousands for wide GQWs (120 MLs) for typical values of the electric field strength ($\pm 100$ kV/cm) and aluminum concentration ($x = 0.3$). Last but not least, the special energy band profile studied here can be used to improve the QCSE characteristics in current quantum well systems, such as those based on nitrides, oxides (ZnO), and SiGe, whenever the confinement energy band profile can be modulated in Gaussian form.


[1] D. A. B. Miller, D. S. Chemla, T. C. Damen, A. C. Gossard, W. Wiegmann, T. H. Wood, and C. A. Burrus, Phys. Rev. Lett. **53**, 2173 (1984).
[2] U. Arad, E. Redmard, M. Shamay, A. Averboukh, S. Levit, and U. Efron, IEEE Photon. Technol. Lett. **15**, 1531 (2003).
[3] C. P. Liu, A. Seeds, J. S. Chadha, P. N. Stavrinou, G. Parry, M. Whitehead, A. B. Krysa, and J. S. Roberts, IEICE Trans. Electron. E **86C**, 1281 (2003).
[4] M. Krames, Progress and future direction of LED technology, paper presented at the Department Energy Workshop Solid State Lighting, Arlington, VA, November 2003.
[5] G. Craford, High power LEDs: Technology trends, applications, and solid state lighting, paper presented at the 4th China Internal Forum Solid-State Lighting (China SSL), Shanghai, China, August 2007.
[6] P. Bhattacharya, *Semiconductor Optoelectronic Devices*, 2nd ed. (Prentice-Hall, Upper Saddle River, NJ, 1997), pp. 452–456.
[7] B. Jalali and S. Fathpour, J. Lightwave Technol. **24**, 4600 (2006).
[8] Y.-H. Kuo, Y. K. Lee, Y. Ge, S. Ren, J. E. Roth, T. I. Kamins, D. A. B. Miller, and J. S. Harris, Nature (London) **437**, 1334 (2005).
[9] T. Takeuchi, S. Sota, M. Katsuragawa, M. Komori, H. Takeuchi, H. Amano, and I. Akasaki, Jpn. J. Appl. Phys. **36**, L382 (1997).
[10] M. Leroux, N. Grandjean, M. Laügt, J. Massies, B. Gil, P. Lefebvre, and P. Bigenwald, Phys. Rev. B **58**, R13371 (1998).
[11] S. F. Chichibu, A. C. Abare, M. S. Minsky, S. Keller, S. B. Fleischer, J. E. Bowers, E. Hu, U. K. Mishra, L. A. Coldren, S. P. DenBaars, and T. Sota, Appl. Phys. Lett. **73**, 2006 (1998).
[12] N. Grandjean, B. Damilano, S. Dalmasso, M. Leroux, M. Laügt, and J. Massies, J. Appl. Phys. **86**, 3714 (1999).
[13] T. Deguchi, K. Sekiguchi, A. Nakamura, T. Sota, R. Matsuo, S. Chichibu, and S. Nakamura, Jpn. J. Appl. Phys. **38**, L914 (1999).
[14] H. M. Hg, Appl. Phys. Lett. **80**, 4369 (2002).
[15] J.-R. Ryou, P. D. Yoder, J. Liu, Z. Lochner, H. Kim, S. Choi, H. J. Kim, and R. D. Dupuis, IEEE J. Sel. Top Quantum Electron. **15**, 1080 (2009).
[16] T. Makino, A. Ohtomo, C. H. Chia, Y. Segawa, H. Koinuma, and M. Kawasaki, Physica E **21**, 671 (2004).
[17] C. Morhain, T. Bretagnon, P. Lefebvre, X. Tang, P. Valvin, T. Guillet, B. Gil, T. Taliercio, M. Teisseire-Doninelli, B. Vinter, and C. Deparis, Phys. Rev. B **72**, 241305(R) (2005).
[18] T. Makino, Y. Segawa, M. Kawasaki, and H. Koinuma, Semicond. Sci. Technol. **20**, S78 (2005).
[19] T. Bretagnon, P. Lefebvre, T. Guillet, T. Taliercio, B. Gil, and C. Morhain, Appl. Phys. Lett. **90**, 201912 (2007).
[20] T. Makino, Y. Segawa, A. Tsukazaki, A. Ohtomo, and M. Kawasaki, Appl. Phys. Lett. **93**, 121907 (2008).
[21] C. R. Hall, L. V. Dao, K. Koike, S. Sasa, H. H. Tan, M. Inoue, M. Yano, C. Jagadish, and J. A. Davis, Appl. Phys. Lett. **96**, 193117 (2010).
[22] J. Park and Y. Kawakami, Appl. Phys. Lett. **88**, 202107 (2006).
[23] S.-H. Park, J. Park, and E. Yoon, Appl. Phys. Lett. **90**, 023508 (2007).
[24] S.-H. Yen and Y.-K. Kuo, Opt. Commun. **281**, 4735 (2008).
[25] H. Zhao, G Liu, J. Zhang, J. D. Poplawsky, V. Dierolf, and N. Tansu, Opt. Express **19**, A991 (2011).
[26] L. Wang, R. Li, Z. Yang, D. Li, T. Yu, N. Liu, L. Liu, W. Chen, and X. Hu, Appl. Phys. Lett. **95**, 211104 (2009).
[27] Z. Yang, R. Liu, Q. Wei, T. Yu, Y. Zhang, W. Chen, and X. Hu, Appl. Phys. Lett. **94**, 061120 (2009).
[28] S.-H. Han, D.-Y. Lee, H.-W. Shim, G.-C. Kim, Y. S. Kim, S.-T. Kim, S.-J. Lee, C.-Y. Cho, and S.-J. Park, J. Phys. D: Appl. Phys. **43**, 354004 (2010).
[29] D. J. Chadi, Phys. Rev. B **16**, 790 (1977).
[30] P. Vogl, H. P. H. Hjalmarson, and J. D. Dow, J. Phys. Chem. Solids **44**, 365 (1983).
[31] C. Priester, G. Allan, and M. Lannoo, Phys. Rev. B **37**, 8519 (1988).
[32] M. C. Muñoz, V. R. Velasco, and F. García-Moliner, Phys. Rev. B **39**, 1786 (1989); D. A. Contreras-Solorio, V. R. Velasco, and F. García-Moliner, *ibid.* **47**, 4651 (1993); S. Vlaev, V. R. Velasco, and F. García-Moliner, *ibid.* **51**, 7321 (1995).
[33] M. P. López Sancho, J. M. López Sancho, and J. Rubio, J. Phys. F **14**, 1205 (1984); **15**, 851 (1985).
[34] M. Graf and P. Vogl, Phys. Rev. B **51**, 4940 (1995).